

## Attenuation and amplification of the transient current in nanojunctions with time-varying gate potentials

Eduardo C. Cuansing

*Institute of Mathematical Sciences and Physics, University of the Philippines, Los Baños, 4031 Laguna, Philippines*  
*eccuansing@up.edu.ph*

We study charge transport in a source-channel-drain system with a time-varying applied gate potential acting on the channel. We calculate both the current flowing from the source into the channel and out of the channel into the drain. The current is expressed in terms of nonequilibrium Green's functions. These nonequilibrium Green's functions can be determined from the steady-state Green's functions and the equilibrium Green's functions of the free leads. We find that the application of the gate potential can induce current to flow even when there is no source-drain bias potential. However, the direction of the current from the source and the current to the drain are opposite, thereby resulting in no net current flowing within the channel. When a source-drain bias potential is present, the net current flowing to the source and drain can either be attenuated or amplified depending on the sign of the applied gate potential. We also find that the response of the system to a dynamically changing gate potential is not instantaneous, i.e., a relaxation time has to pass before the current settles into a steady value. In particular, when the gate potential is in the form of a step function, the current first overshoots to a maximum value, oscillates, and then settles down to a steady-state value.

*Keywords:* Time-dependent quantum transport, nonequilibrium Green's functions, nanodevices

PACS numbers: 72.10.Bg, 73.23.-b, 73.50.Bk, 05.10.-a

### 1. Introduction

The relentless pursuit of miniaturization in electronics will eventually lead to devices consisting of just a few atoms and molecules, with charge carriers limited to move within reduced dimensions.<sup>1,2,3</sup> Given the small system sizes involved in molecular devices, a full quantum-mechanical treatment is necessary in order for us to correctly understand and predict the behavior and properties of the system. Several groups have experimentally created molecular junctions and measured the transport properties of these devices,<sup>4,5,6</sup> including the appearance of negative differential resistance,<sup>7</sup> Coulomb blockade,<sup>8</sup> and Kondo resonances.<sup>8,9</sup> An important issue in molecular electronics is to determine the response of the system to time-varying forces and system parameters. Experiments have been done to measure the dynamic current in a quantum dot system with a time-varying bias potential,<sup>10,11</sup> in the switching of the bond angle in bistable atoms,<sup>12</sup> in the controlled emission of electrons from a nanoscale tip,<sup>13</sup> and in the application of a gate potential to a

Wigner solid on liquid helium.<sup>14</sup> These experiments show that whenever a change occurs in the system, the response is not instantaneous, there is an initial overshoot, and current oscillations persist for some time before approaching a steady-state value. Theoretical approaches to model the response of quantum systems to time-dependent changes include time-dependent density functional theory,<sup>15,16,17,18,19</sup> Floquet theory,<sup>20,21,22,23</sup> density matrix renormalization group method,<sup>24</sup> quantum Master equation,<sup>25,26</sup> Kadanoff-Baym equations,<sup>27,28</sup> and nonequilibrium Green's functions method.<sup>29,30,31,32,33,34,36,37</sup> The nonequilibrium Green's functions method, in particular, is highly suitable in quantum transport calculations of devices that can be partitioned into a source-channel-drain configuration.

Nonequilibrium Green's functions are functions of two time variables. In the steady-state regime, the system satisfies time-translation invariance and thus, one of the time variables can be integrated out and the Fourier transform of the Green's functions can be utilized to re-express the functions in the energy domain.<sup>35</sup> For the full time-dependent behavior, including during the transient regime where time-translation invariance is no longer satisfied, the Green's functions must be expressed in either two time variables, two energy variables, or a combination of one time and one energy variables. Two-time nonequilibrium Green's functions have been used to study the response of a quantum dot device to a pulsed source-drain bias potential<sup>29,36,38</sup>, including an analytically exact solution for Lorentzian linewidths,<sup>37</sup> and a nano-relay where the coupling between parts of the device is varied in time.<sup>39</sup> Double-energy nonequilibrium Green's functions have been used to study the response of a carbon nanotube transistor to a time-dependent gate potential,<sup>40</sup> in resonant-tunneling devices,<sup>41</sup> and in photon-assisted transport.<sup>42</sup> Nonequilibrium Green's functions expressed as functions of a combination of one time and one energy variables have been used to study the thermopower in a quantum dot device with a time-dependent gate voltage.<sup>43</sup> Recently, an energy-resolved self-energies approximation coupled with an auxiliary-mode expansion scheme has been developed to eliminate one of the time-dependence of the two-time nonequilibrium Green's functions.<sup>44</sup> This scheme has been used to calculate the time-dependent current in quantum dot systems in the presence of electron-electron<sup>45</sup> and electron-phonon<sup>46</sup> interactions. In this paper, we determine the two-time nonequilibrium Green's functions directly to investigate the dynamic response of a source-channel-drain device to a time-varying gate potential. We do not calculate the nonequilibrium Green's functions in the energy domain to avoid transforming these functions back to the time domain. Such transformations could entail unphysical Gibbs oscillations in time that must be carefully removed.<sup>47</sup>

This paper is organized as follows. In Sec. 2, we model a source-channel-drain system with a channel containing a single site and a time-varying gate potential is acting on that channel. Expressions for the electron and energy current in terms of nonequilibrium Green's functions are derived. In Sec. 3, the nonequilibrium Green's functions are determined in terms of the steady-state Green's functions and the

equilibrium Green's functions of the free leads. In Sec. 4, we show the results of our calculations for various forms of the gate potential. The summary and conclusion are stated in Sec. 5.

## 2. Model

Shown in Fig. 1 is an illustration of the source-channel-drain device. The channel consists of a single site, labeled 1, where a time-varying gate potential  $V_g(t)$  is present. The left and right leads are semi-infinite linear chains with the source as the left lead and the drain as the right lead. The source-drain bias is a constant  $V_b$ .

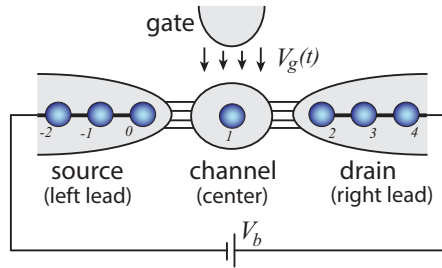


Fig. 1. Illustration of the source-channel-drain device with a single-site channel and a time-varying applied gate potential  $V_g(t)$ . The left and right leads are semi-infinite linear chains.  $V_b$  is the source-drain bias potential. Sites are labeled consecutively.

We model the system using the tight-binding approximation. The total Hamiltonian is  $H = H^L + H^R + H^C + H^{LC} + H^{RC}$ . The Hamiltonian for the left and right leads are

$$\begin{aligned} H^L &= \sum_k \varepsilon_k^L a_k^\dagger a_k + \sum_{k < j} v_{kj}^L (a_k^\dagger a_j + a_j^\dagger a_k), \\ H^R &= \sum_k \varepsilon_k^R b_k^\dagger b_k + \sum_{k < j} v_{kj}^R (b_k^\dagger b_j + b_j^\dagger b_k), \end{aligned} \quad (1)$$

where  $a_k^\dagger$  ( $a_k$ ) and  $b_k^\dagger$  ( $b_k$ ) are the creation (annihilation) operators at site  $k$  in the left and right leads, respectively, the  $\varepsilon_k^L$  and  $\varepsilon_k^R$  are the on-site energies at site  $k$ , the  $v_{kj}^L$  and  $v_{kj}^R$  are the hopping parameters for nearest-neighbor sites  $k$  and  $j$ , and the sums are over all the sites in the leads. The Hamiltonian for the channel can be separated into stationary and time-varying parts, i.e.,  $H^C = H_0^C + H^C(t)$ , where  $H_0^C = \varepsilon_1^C c_1^\dagger c_1$  and  $H^C(t) = U(t) c_1^\dagger c_1$ , where  $c_1^\dagger$  and  $c_1$  are the creation and annihilation operators at site 1 in the channel, the real-valued  $U(t) = -qV_g(t)$  is due to the time-varying potential that the gate exerts on the site in the channel, and  $q$  is the electron charge. The Hamiltonian for the couplings between the leads

and the channel are

$$H^{\text{LC}} = v_{01}^{\text{LC}} (a_0^\dagger c_1 + c_1^\dagger a_0), \quad (2)$$

$$H^{\text{RC}} = v_{21}^{\text{RC}} (c_1^\dagger b_2 + b_2^\dagger c_1), \quad (3)$$

where the coupling parameters  $v^{\text{LC}} = v^{\text{CL}}$  and  $v^{\text{RC}} = v^{\text{CR}}$  are symmetric. The current flowing out of the left lead can be determined from the changes in the number operator,  $N^{\text{L}} = \sum_k a_k^\dagger a_k$ , of the left lead:

$$I^{\text{L}}(t) = \left\langle -q \frac{dN^{\text{L}}}{dt} \right\rangle = -\frac{iq}{\hbar} \langle [H, N^{\text{L}}] \rangle = 2q \text{Re} \left[ v_{01}^{\text{LC}} G_{10}^{\text{CL},<}(t, t) \right], \quad (4)$$

where the negative sign in the first equality implies the sign of  $I^{\text{L}}$  is positive if the current is flowing out of the left lead and  $\text{Re}[\cdot]$  means taking the real part. The lesser nonequilibrium Green's function is defined as  $G_{10}^{\text{CL},<}(t_1, t_2) = \frac{i}{\hbar} \langle a_0^\dagger(t_2) c_1(t_1) \rangle$ . The third equality in Eq. (4) is derived using the fermion anti-commutation relation  $\{a_j, a_k^\dagger\} = \delta_{jk}$ . Similarly, the current flowing into the right lead is

$$I^{\text{R}}(t) = \left\langle q \frac{dN^{\text{R}}}{dt} \right\rangle = -2q \text{Re} \left[ v_{21}^{\text{RC}} G_{12}^{\text{CR},<}(t, t) \right], \quad (5)$$

where  $G_{12}^{\text{CR},<}(t_1, t_2) = \frac{i}{\hbar} \langle b_2^\dagger(t_2) c_1(t_1) \rangle$  and the sign of  $I^{\text{R}}$  is positive if current is flowing into the right lead. For both the left and right leads, therefore, the sign of the current is positive whenever it is flowing from the left to the right.

Another important dynamical variable is the amount of energy that the electrons carry across the device, i.e., the heat due to electron flow. This can be calculated from the rate of change of the lead Hamiltonian. The heat resulting from the electrons flowing out of the left lead is

$$Q^{\text{L}}(t) = -\left\langle \frac{dH^{\text{L}}}{dt} \right\rangle = 2 \text{Re} \left[ (\varepsilon_0^{\text{L}} v_{01}^{\text{LC}} + v_{00}^{\text{L}} v_{01}^{\text{LC}}) G_{10}^{\text{CL},<}(t, t) \right] \quad (6)$$

while the heat due to electrons flowing into the right lead is

$$Q^{\text{R}}(t) = \left\langle \frac{dH^{\text{R}}}{dt} \right\rangle = -2 \text{Re} \left[ (\varepsilon_2^{\text{R}} v_{21}^{\text{RC}} + v_{22}^{\text{R}} v_{21}^{\text{RC}}) G_{12}^{\text{CR},<}(t, t) \right]. \quad (7)$$

Notice from the above expressions that the dynamics of the heat flowing into or out of the leads simply follow, up to constant factors, the dynamics of the flow of electrons into or out of those leads. Note, however, that the dynamics considered here is due solely to the time-varying gate potential. If the couplings between the leads and the channel are also varied, heat flow may not follow the dynamics of the flow of the electronic current.<sup>48,49</sup> Furthermore, the heat resulting from the flow of phonons and the heat due to electron-phonon interactions are not incorporated in Eqs. (6) and (7).

### 3. Nonequilibrium Green's Functions

The Green's functions are calculated based on the switch-on process described in Fig. 2. At time  $t \rightarrow -\infty$  the leads and the channel are uncoupled. The leads are considered to be separately in equilibrium at their respective temperatures and chemical potentials at this time. The couplings are then adiabatically switched on such that at time  $t = 0$  they have reached their full values. The system is thus at a steady state at this time. The gate potential is then switched on at time  $t = 0$ .

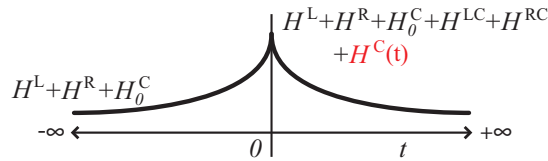


Fig. 2. Illustration of how components of the total Hamiltonian are switched on in time.

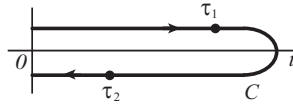


Fig. 3. Illustration of the Keldysh contour for time  $t$ .  $\tau_1$  and  $\tau_2$  are contour time variables and the arrows show the direction of contour ordering.

The lesser nonequilibrium Green's functions can be determined from the Keldysh formalism where time is extended into the complex plane.<sup>29,32,33,34</sup> We first define the contour-ordered Green's function  $G_{10}^{\text{CL}}(\tau_1, \tau_2) = -\frac{i}{\hbar} \langle T_c c_1(\tau_1) a_0^\dagger(\tau_2) \rangle$ , where  $T_c$  is the contour-ordering operator and  $\tau_1$  and  $\tau_2$  are contour time variables on the Keldysh contour, as shown in Fig. 3. To calculate the Green's function we separate the total Hamiltonian into a stationary and a time-varying part,  $H = H_0 + H^C(t)$ , and the transformation from the Heisenberg picture to the Interaction picture gives

$$G_{10}^{\text{CL}}(\tau_1, \tau_2) = -\frac{i}{\hbar} \left\langle T_c e^{-\frac{i}{\hbar} \int_C H^C(\tau') d\tau'} c_1(\tau_1) a_0^\dagger(\tau_2) \right\rangle_0 \quad (8)$$

where the  $\langle \dots \rangle_0$  implies an ensemble average taken with respect to the steady state. This Green's function can be expanded perturbatively using diagrammatic techniques.

Shown in Fig. 4 are the diagram representations of the contour-ordered Green's functions needed for the expansion of Eq. (8). And shown in Fig. 5 is the diagrammatic expansion for  $G_{10}^{\text{CL}}(\tau_1, \tau_2)$ .

From Fig. 5, the resulting iterative Dyson equation is

$$G_{10}^{\text{CL}}(\tau_1, \tau_2) = G_{10,0}^{\text{CL}}(\tau_1, \tau_2) + \int_C d\tau' G_{11,0}^{\text{CC}}(\tau_1, \tau') U_1(\tau') G_{10}^{\text{CL}}(\tau', \tau_2), \quad (9)$$

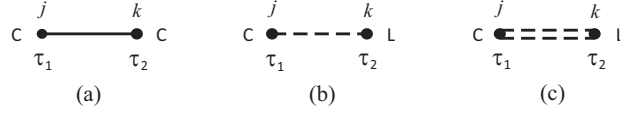


Fig. 4. Diagram representations of contour-ordered Green's functions. The diagrams represent (a)  $G_{jk,0}^{CC}(\tau_1, \tau_2)$ , (b)  $G_{jk,0}^{CL}(\tau_1, \tau_2)$ , and (c)  $G_{jk}^{CL}(\tau_1, \tau_2)$ . The subscript 0 indicates a steady-state Green's function.

Fig. 5. The perturbation expansion of  $G_{jk}^{CL}(\tau_1, \tau_2)$  in terms of the steady-state Green's functions. Each vertex (a crossed dot) represents a  $U(\tau)$ .

where the integral is along the Keldysh contour, the subscript 0 indicates a steady-state Green's function, and the center steady-state Green's function  $G_{jk}^{CC}(\tau_1, \tau_2) = -\frac{i}{\hbar} \langle T_c c_j(\tau_1) c_k^\dagger(\tau_2) \rangle$ . To return the contour-time variables back to the real-time axis, we apply analytic continuation and Langreth's theorem.<sup>31</sup> The retarded and advanced Green's functions become

$$G_{10}^{CL,\gamma}(t_1, t_2) = G_{10,0}^{CL,\gamma}(t_1 - t_2) + \int_0^t dt' G_{11,0}^{CC,\gamma}(t_1 - t') U_1(t') G_{10}^{CL,\gamma}(t', t_2), \quad (10)$$

where  $\gamma = r$  and  $a$ , i.e., the retarded and advanced Green's functions, respectively. For the lesser Green's function, following Langreth's theorem

$$\begin{aligned} G_{10}^{CL,<}(t_1, t_2) &= G_{10,0}^{CL,<}(t_1, t_2) + \int_0^t dt' G_{11,0}^{CC,r}(t_1, t') U_1(t') G_{10}^{CL,<}(t', t_2) \\ &\quad + \int_0^t dt' G_{11,0}^{CC,<}(t_1, t') U_1(t') G_{10}^{CL,a}(t', t_2). \end{aligned} \quad (11)$$

Notice that the second term in the right-hand side of the equation contains  $G_{10}^{CL,<}$ . This can be solved by iteratively substituting Eq. (11) whenever  $G_{10}^{CL,<}$  appears in the equation. For example, the first iteration is

$$\begin{aligned} G_{10}^{CL,<}(t_1, t_2) &= G_{10,0}^{CL,<}(t_1, t_2) + \int_0^t dt' G_{11,0}^{CC,r}(t_1, t') U_1(t') G_{10}^{CL,<}(t', t_2) \\ &\quad + \int_0^t dt' \int_0^t dt'' G_{11,0}^{CC,r}(t_1, t') U_1(t') G_{11,0}^{CC,r}(t', t'') U_1(t'') G_{10}^{CL,<}(t'', t_2) \\ &\quad + \int_0^t dt' \int_0^t dt'' G_{11,0}^{CC,r}(t_1, t') U_1(t') G_{11,0}^{CC,<}(t', t'') U_1(t'') G_{10}^{CL,a}(t'', t_2) \\ &\quad + \int_0^t dt' G_{11,0}^{CC,<}(t_1, t') U_1(t') G_{10}^{CL,a}(t', t_2), \end{aligned} \quad (12)$$

where  $G_{10}^{\text{CL},<}$  appears in the third term of the right-hand side of the equation. After we keep on iteratively substituting Eq. (11) and combining terms, we get

$$\begin{aligned} G_{10}^{\text{CL},<}(t_1, t_2) &= G_{10,0}^{\text{CL},<}(t_1, t_2) + \int_0^t dt' G_{11}^{\text{CC},r}(t_1, t') U_1(t') G_{10,0}^{\text{CL},<}(t', t_2) \\ &+ \int_0^t dt' G_{11,0}^{\text{CC},<}(t_1, t') U_1(t') G_{10}^{\text{CL},a}(t', t_2) \\ &+ \int_0^t dt' \int_0^t dt'' G_{11}^{\text{CC},r}(t_1, t') U_1(t') G_{11,0}^{\text{CC},<}(t', t'') U_1(t'') G_{10}^{\text{CL},a}(t'', t_2). \end{aligned} \quad (13)$$

To determine  $G_{10}^{\text{CL},<}$  then the expressions for the center Green's functions  $G_{11}^{\text{CC},<}$ ,  $G_{11}^{\text{CC},r}$ ,  $G_{11}^{\text{CC},a}$ , and their corresponding steady-state versions are needed. The nonequilibrium CC Green's functions can be determined by following the above same procedure. The result is in the same form as Eq. (10) and Eq. (13) except for the replacement of all of the L superscripts with a C and all of the 0 site labels with a 1. In addition, the same procedure can be employed to find the expression for  $G_{12}^{\text{CR},<}$  for the right current in Eq. (5). The result is again of the same form as Eqs. (10) and (13) except for the replacement of all of the L superscripts with an R and all of the 0 site labels with a 2.

The integrals in Eq. (13) for  $G_{10}^{\text{CL},<}(t_1, t_2)$  require not just the steady-state Green's functions but also the non-steady-state retarded and advanced Green's functions. We thus determine the retarded and advanced Green's functions first. Notice that these Green's functions are in iterative integral equations, as shown in Eq. (10), and can be solved following a numerical procedure. Equation (10) is in the form

$$f(t_a, t_b) = f_0(t_a, t_b) + \int_{t_1}^{t_N} f_0(t_a, t') U(t') f(t', t_b) dt', \quad (14)$$

where  $t_1 \leq t_a, t_b \leq t_N$ . Replacing the integral with the corresponding expression using numerical integration

$$f(t_a, t_b) = f_0(t_a, t_b) + \Delta t \cdot \sum_{i=1}^N c_i f_0(t_a, t_i) U(t_i) f(t_i, t_b), \quad (15)$$

where the  $c_i$  are the numerical integration coefficients. A linear problem can then be constructed in the form  $A\vec{x} = \vec{b}$ , where

$$A = \begin{pmatrix} 1 - \Delta t c_1 f_0(t_1, t_1) U(t_1) & -\Delta t c_2 f_0(t_1, t_2) U(t_2) & \cdots \\ -\Delta t c_1 f_0(t_2, t_1) U(t_1) & 1 - \Delta t c_2 f_0(t_2, t_2) U(t_2) & \cdots \\ \vdots & \vdots & \ddots \end{pmatrix}, \quad (16)$$

is an  $N \times N$  matrix,

$$\vec{x} = \begin{pmatrix} f(t_1, t_b) \\ f(t_2, t_b) \\ \vdots \\ f(t_N, t_b) \end{pmatrix}, \text{ and } \vec{b} = \begin{pmatrix} f_0(t_1, t_b) \\ f_0(t_2, t_b) \\ \vdots \\ f_0(t_N, t_b) \end{pmatrix}, \quad (17)$$

are  $N$ -dimensional column vectors whose sizes depend on the length of the time interval from  $t_1$  to  $t_N$  and the time step  $\Delta t$ . The solution is calculated numerically from the inverse of  $A$ , i.e.,  $\vec{x} = A^{-1}\vec{b}$ , using LU decomposition.<sup>47</sup> Once the retarded and advanced non-steady-state Green's functions are determined, the integrals in Eq. (13) can be calculated numerically using the method of quadratures.<sup>47</sup>

The steady-state Green's functions can be built from the adiabatic switch-on of the coupling between the leads and the channel. Since time-translation invariance is satisfied in the steady state, the Green's functions depend only on the difference between its two time variables. The Fourier transforms of these functions into the energy domain are therefore well-defined with the resulting CC steady-state Green's functions as

$$G_{11,0}^{\text{CC},r}(E) = \left[ (E + i\eta) - \varepsilon_1^{\text{C}} - \Sigma_{11}^{\text{C},r}(E) \right]^{-1}, \quad (18)$$

$$G_{11,0}^{\text{CC},a}(E) = \left( G_{11,0}^{\text{CC},r}(E) \right)^*, \quad (19)$$

$$G_{11,0}^{\text{CC},<}(E) = G_{11,0}^{\text{CC},r}(E) \Sigma_{11}^{\text{C},<}(E) G_{11,0}^{\text{CC},a}(E), \quad (20)$$

where the self-energies are

$$\Sigma_{11}^{\text{C},\alpha} = v_{10}^{\text{CL}} g_{00}^{\text{L},\alpha}(E) v_{01}^{\text{LC}} + v_{12}^{\text{CR}} g_{22}^{\text{R},\alpha}(E) v_{21}^{\text{RC}}, \quad (21)$$

where  $\alpha = \text{r, a, and } <$ , and the  $g_{00}^{\text{L},\alpha}(E)$  and  $g_{22}^{\text{R},\alpha}(E)$  are the equilibrium Green's functions for the left and right leads, respectively. The CL steady-state Green's functions are

$$G_{10,0}^{\text{CL},r}(E) = G_{11,0}^{\text{CC},r}(E) v_{10}^{\text{CL}} g_{00}^{\text{L},r}(E), \quad (22)$$

$$G_{10,0}^{\text{CL},a}(E) = \left( G_{10,0}^{\text{CL},r}(E) \right)^*, \quad (23)$$

$$G_{10,0}^{\text{CL},<}(E) = G_{11,0}^{\text{CC},r}(E) v_{10}^{\text{CL}} g_{00}^{\text{L},<}(E) + G_{11,0}^{\text{CC},r}(E) \Sigma_{11}^{\text{C},<}(E) G_{10,0}^{\text{CL},a}(E). \quad (24)$$

The CR steady-state Green's functions have the same form as those in Eqs. (22) to (24) except for the replacement of the L superscripts with R and the 0 site labels with 2. Once the steady-state Green's functions in the energy domain have been determined, their Fourier transforms into the time domain are required for the calculation of the full time-dependent nonequilibrium Green's functions.

The equilibrium Green's functions for the left and right leads can be determined



from the solution of the equations of motion of the particles. For the left lead,

$$g_{00}^{L,r}(E) = 2 \frac{(E + i\eta) - \varepsilon_0^L}{v^2} \pm 2i \frac{\sqrt{v^2 - (\varepsilon_0^L - E)^2}}{v^2}, \quad (25)$$

$$g_{00}^{L,a}(E) = \left(g_{00}^{L,r}(E)\right)^*, \quad (26)$$

$$g_{00}^{L,<}(E) = -f^L(E) \left(g_{00}^{L,r}(E) - g_{00}^{L,a}(E)\right), \quad (27)$$

where  $v$  is the hopping parameter between site 0 and site  $-1$  in the left lead and  $f^L(E) = [e^{(E - \mu_L)/k_B T_L} + 1]^{-1}$  is the Fermi-Dirac distribution function, where  $\mu_L$  is the chemical potential and  $T_L$  is the temperature of the left lead, respectively. The expressions for the equilibrium Green's functions for the right lead are of the same form as Eqs. (25) to (27).

To calculate, therefore, the left and right currents in Eqs. (4) and (5), respectively, the corresponding nonequilibrium Green's functions  $G_{10}^{CL,<}(t_1, t_2)$  and  $G_{12}^{CR,<}(t_1, t_2)$  are needed. These Green's functions can be expressed in terms of the steady-state Green's functions, i.e., Eqs. (10) and (13), and, in turn, the steady-state Green's functions can be expressed in terms of the equilibrium Green's functions, i.e., Eqs. (18) to (24). The equilibrium Green's functions are calculated from Eqs. (25) to (27).

#### 4. Numerical Results

In our numerical calculations we use the following parameters:  $\varepsilon^L = \varepsilon^R = \varepsilon^C = 0$  and  $v^L = v^R = v^{LC} = v^{RC} = 2$  eV. For the left lead  $\mu_L = E_F$  while for the right lead  $\mu_R = E_F - v_b$ , where we set the Fermi energy  $E_F = 0$  and  $v_b$  is the source-drain bias potential. Both the left and right leads have the same temperature  $T_L = T_R = 300$  K. We use a time step of  $\Delta t = 0.05$  fs.

Shown in Fig. 6 are plots of the current flowing out of the left lead as functions of time,  $I^L(t)$ , and frequency,  $I^L(f)$ . The  $I^L(f)$  is the Fourier transform of its time-domain counterpart and are calculated using the FFTW software package.<sup>50</sup> The gate potential is switched on in the form of a Heaviside step function at time  $t = 0$ . There is no source-drain bias potential across the device, i.e.,  $v_b = 0$ . The current, therefore, should not flow without the action of the gate potential. At the transient regime as the gate potential is switched on, the current takes time to react, overshoots to a large value, and then oscillates down to a steady value. The height of the overshoot and the amplitude of the oscillations depend on the strength of the gate potential. In the plot of  $|I^L(f)|^2$  as a function of the frequency shown in Fig. 6(b), there is a sharp peak around  $f = 0$  indicating the DC component of the current. There are two other peaks showing up at  $\pm 0.7 \times 10^{15}$  Hz. These peaks correspond to the frequency of oscillation of the current as it settles down from the transient to the steady-state regime.

Shown in Fig. 7 are the plots of the left and right current for a pulsed gate potential (represented by the dash lines) and there is no source-drain bias potential.

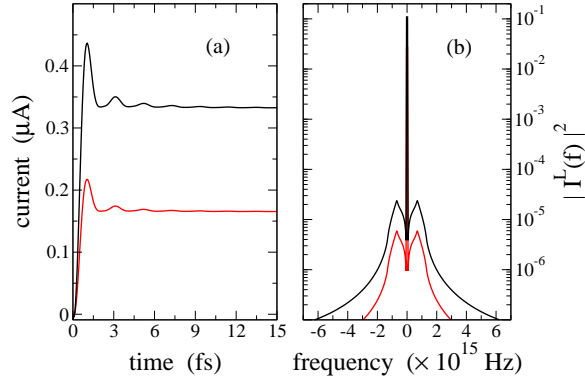


Fig. 6. (a) The current from the left lead  $I^L(t)$  as a function of time when the gate potential is switched-on as a step function at time  $t = 0$ . For the time interval up to 15 fs and a time step of  $\Delta t = 0.05$  fs, the corresponding matrix  $A$  in Eq. (16) has size  $N^2 = 90000$ . (b) Semi-log plot of  $|I^L(f)|^2$  as a function of the frequency  $f$  where  $I^L(f)$  is the Fourier transform of the current  $I^L(t)$ . For both figures, the gate potentials are 0.1 eV (dark line) and 0.05 eV (light line, red online). There is no source-drain bias potential and both leads have the same temperature  $T = 300$  K.

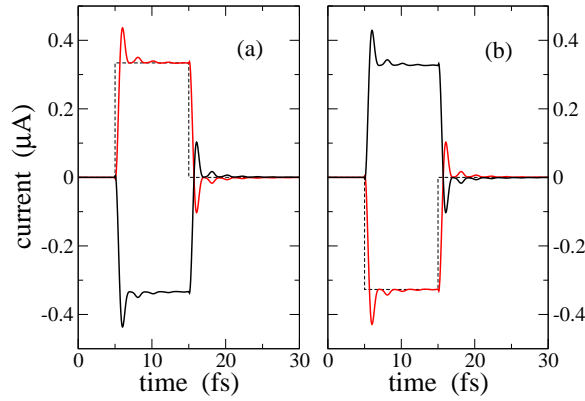


Fig. 7. The current from the left lead  $I^L(t)$  (light line, red online) and right lead  $I^R(t)$  (dark line) when a pulsed gate potential (represented by the dash line) acts on the channel. The gate potential in (a) is 0.1 eV while in (b) it is  $-0.1$  eV during the pulse. There is no source-drain bias potential. The corresponding matrix  $A$  has size  $N^2 = 360000$ .

The pulse is on between  $t = 5$  fs and  $t = 15$  fs. Notice that when the gate potential is  $+0.1$  eV the direction of the left current is to the right while the direction of the right current is to the left, as shown in Fig. 7(a). In contrast, when the gate potential has the opposite sign, the directions of the currents are reversed, as shown in Fig. 7(b). Note that the charge carriers are electrons and thus a positive gate potential is attractive to the particles while a negative gate potential is repulsive. When the gate potential is positive, therefore, electrons from both the left and right leads flow into the channel. The opposite direction happens when the gate potential is negative. Notice too that the response of the current to a sudden change in the

gate potential is to overshoot, oscillate, and eventually settle down to a steady value. The form of the current during the downward step pulse is a mirror reflection of the form during the upward step pulse. Since there is no applied source-drain bias potential, and therefore no preferred direction, the symmetry in the dynamics of the current between the upward and downward step pulses is expected. This symmetry is not satisfied when the linewidths of the leads are in the wide-band limit<sup>29</sup> or in a finite interval<sup>36,37</sup> where not all energy levels in the leads are available for the electrons to propagate through.

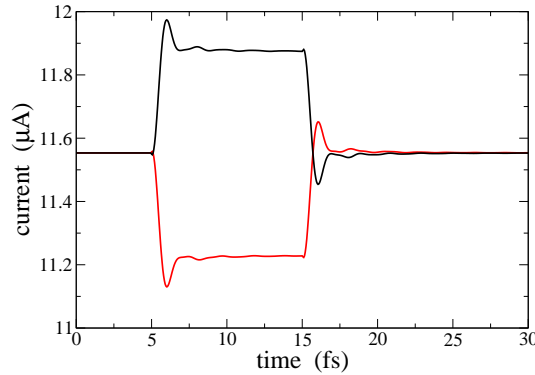


Fig. 8. The left current (light line, red online) and right current (dark line) when a pulsed  $-0.1$  eV gate potential acts on the channel. The source-drain bias potential is  $0.3$  eV.

Since the effect of the gate potential is to induce current to flow in opposite directions between the left and right leads, a gate potential without an accompanying source-drain bias potential will not result in a net flow of current. Shown in Fig. 8 is the current when a  $0.3$  eV bias potential is applied across the device and a pulsed  $-0.1$  eV gate potential acts on the channel. The pulse gate potential is switched on at  $t = 5$  fs and off at  $t = 15$  fs. Both the left and right currents have the same steady values before the pulse is switched on. Also, for long times after the pulse has been switched off, both the left and right currents have the same steady values. These steady values are consistent with the steady-state current values calculated using the Landauer formula.<sup>51</sup> When the gate potential is on, the current flowing out of the left lead is attenuated while that flowing into the right lead is amplified.

Shown in Fig. 9 is the current flowing into the right lead when the gate potential is a series of rectangular pulses. The widths of the pulses are  $3$  fs, shown in Fig. 9(a), and  $1$  fs, shown in Fig. 9(b). There is no source-drain bias potential. In the figures, the current overshoots whenever an upward or a downward pulse occurs. In a  $3$  fs pulse the width is long enough for the current to make at least one oscillation after an overshoot. In the  $1$  fs pulse the width is too short for the current to complete an oscillation. Also notice that the height of the overshoots increases for the first few successive pulses. Because the gate potential is varying rapidly, the current does not

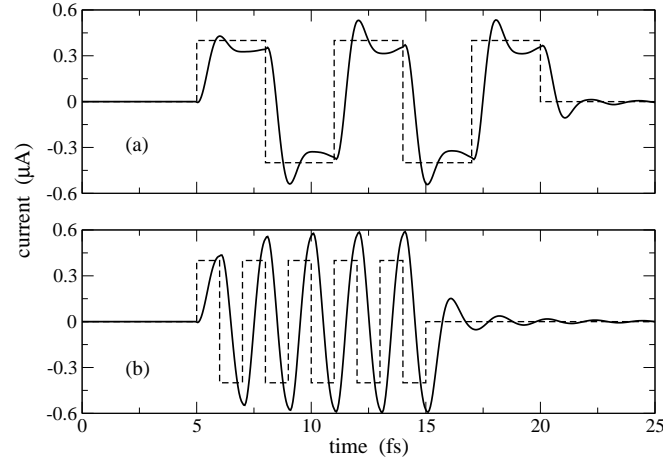


Fig. 9. The right current in a series of 0.3 eV rectangular gate pulses (represented by the dash lines) of alternating signs with widths (a) 3 fs and (b) 1 fs. There is no source-drain bias potential.

have enough time to reach a steady-state value and ends up overshooting back and forth trying to catch up with the pulsing gate potential.

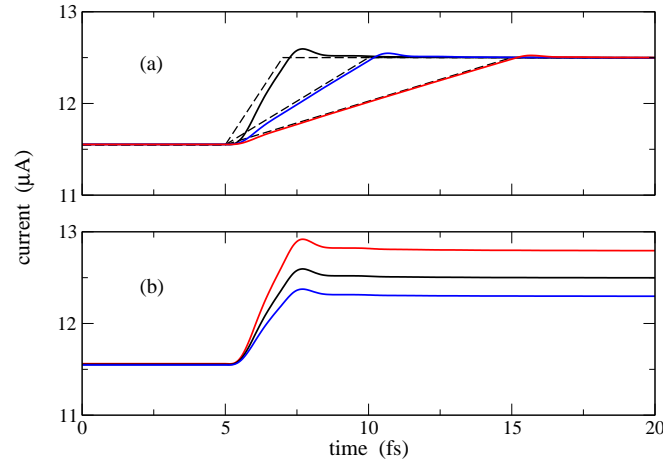


Fig. 10. The right current when the gate potential is switched on in the form of a ramp (represented by the dash lines). The gate potential is switched on at  $t = 5$  fs and then gradually decreased to  $-0.3$  eV. In (a), the widths of the potential ramp are 2 fs (dark line), 5 fs (lighter line, blue online), and 10 fs (light line, red online). In (b), the width of the ramp is 2 fs while the lead-channel couplings are varied: 2 eV (dark line), 2.2 eV (lighter line, blue online), and 1.8 eV (light line, red online). The source-drain bias potential is 0.3 eV.

The speed of the switch-on of the gate potential affects the height of the current overshoot and the accompanying oscillations. Shown in Fig. 10 is the right current

when the gate potential is switched on gradually in the form of a ramp. In Fig. 10(a) the width of the switch-on is varied from 2 fs to 5 fs and then to 10 fs. For the 2 fs ramp, the current rises behind the gate potential, overshoots once the gate potential abruptly changes direction, and the oscillates until it reaches a steady value. In the slightly softer 5 fs ramp, the current more closely follows the rising gate potential but still overshoots, although with a shorter amplitude, when the gate potential changes direction. For the soft 10 fs ramp, the current almost follows the rising gate potential and only softly overshoots when the gate potential changes direction.

In Fig. 10(b) the width of the gate potential ramp is maintained at 2 fs and we vary the leads-channel coupling parameters from  $v^{\text{LC}} = v^{\text{RC}} = 1.8$  eV to 2 eV and then to 2.2 eV. Recall that for the leads, we use  $v^{\text{L}} = v^{\text{R}} = 2$  eV. A different leads-channel coupling parameter implies using a channel that is different from the leads. Notice that one of the results of changing the leads-channel coupling is to vary the steady-state value of the current. The initial line before the switch-on, i.e., when  $t < 5$  fs, are actually three lines that do not exactly have the same values. The gate subsequently amplifies these differences as it is switched on. We also see that a stronger leads-channel coupling would reduce the height of the current overshoot as the gate potential changes direction.

## 5. Summary and Conclusion

We model a source-channel-drain system with a channel containing a single site. A time-varying gate potential is acting on the channel thereby making the on-site energy of the site in the channel also vary in time. The electron current flowing from the source (the left lead) and also the current flowing into the drain (the right lead) can be expressed in terms of nonequilibrium Green's functions. These nonequilibrium Green's functions can be expressed in terms of the integrals of steady-state Green's functions. Furthermore, the steady-state Green's functions can be written in terms of the integrals of the equilibrium Green's functions in the leads. The equilibrium Green's functions are calculated from the equation of motion of the free leads.

The response of the device to a change in the gate potential is not instantaneous. A relaxation time has to pass before the current settles down to a steady value. In the case when the gate potential is in the form of a step function, the current overshoots to a maximum value, oscillates, and then settles down to a steady-state value. The amplitude of the overshoot and the oscillations depend on the strength and how fast the gate potential is changing. The faster the gate potential is changing, the higher are the resulting amplitudes in the transient current.

Electrons would flow when a time-varying gate potential is present even when there is no source-drain bias potential. However, the direction of current flow is opposite between the left and right leads, leading to no net current flow in the channel. When a bias potential is present, the current flowing across the channel can be attenuated or amplified depending on the sign of the gate potential.

## Acknowledgments

The author is grateful to Jian-Sheng Wang, Gengchiao Albert Liang, Francis Bayocboc, and Christian Laurio for insightful discussions. This work is funded by the UP System Enhanced Creative Work and Research Grant (ECWRG-2015-2-025).

1. A. Aviram and M. A. Ratner, *Chem. Phys. Lett.* **29**, 277 (1974).
2. J. R. Heath and M. A. Ratner, *Phys. Today* **56**, 43 (2003).
3. N. J. Tao, *Nature Nanotechnol.* **1**, 173 (2006).
4. J. Reichert, R. Ochs, D. Beckmann, H. B. Weber, M. Mayor, and H. v. Löhneysen, *Phys. Rev. Lett.* **88**, 176804 (2002).
5. X. D. Cui, A. Primak, X. Zarate, J. Tomfohr, O. F. Sankey, A. L. Moore, T. A. Moore, D. Gust, G. Harris, and S. M. Lindsay, *Science* **294**, 571 (2001).
6. S. Kubatkin, A. Danilov, M. Hjort, J. Comil, J.-L. Brédas, N. Stuhr-Hansen, P. Hedegård, and T. Bjørnholm, *Nature (London)* **425**, 698 (2003).
7. N. P. Guisinger, M. E. Greene, R. Basu, A. S. Baluch, and M. C. Hersam, *Nano Lett.* **4**, 55 (2004).
8. J. Park, A. N. Pasupathy, J. I. Goldsmith, C. Chang, Y. Yaish, J. R. Petta, M. Rinkoski, J. P. Sethna, H. D. Abruña, P. L. McEuen, and D. C. Ralph, *Nature (London)* **417**, 722 (2002).
9. W. Liang, M. P. Shores, M. Bockrath, J. R. Long, and H. Park, *Nature (London)* **417**, 725 (2002).
10. W.-T. Lai, D. M. T. Kuo, and P.-W. Li, *Physica E* **41**, 886 (2009).
11. W. Lu, Z. Ji, L. Pfeiffer, K. W. West, and A. J. Rimberg, *Nature (London)* **423**, 422 (2003).
12. A. Sweetman, S. Jarvis, R. Danza, J. Bamidele, S. Gangopadhyay, G. A. Shaw, L. Kantorovich, and P. Moriarty, *Phys. Rev. Lett.* **106**, 136101 (2011).
13. M. Krüger, M. Schenk, and P. Hommelhoff, *Nature (London)* **475**, 78 (2011).
14. D. G. Rees, N. R. Beysengulov, J.-J. Lin, and K. Kono, *Phys. Rev. Lett.* **116**, 206801 (2016).
15. E. Runge and E. K. U. Gross, *Phys. Rev. Lett.* **52**, 997 (1984).
16. G. Stefanucci and C.-O. Almbladh, *Phys. Rev. B* **69**, 195318 (2004).
17. N. Bushong, N. Sai, and M. Di Ventra, *Nano Lett.* **5**, 2569 (2005).
18. S. Kurth, G. Stefanucci, E. Khosravi, C. Verdozzi, and E. K. U. Gross, *Phys. Rev. Lett.* **104**, 236801 (2010).
19. K. Varga, *Phys. Rev. B* **83**, 195130 (2011).
20. M. Moskalets and M. Büttiker, *Phys. Rev. B* **66**, 205320 (2002).
21. S. Kohler, J. Lehmann, and P. Hänggi, *Phys. Rep.* **406**, 379 (2005).
22. L. Arrachea and M. Moskalets, *Phys. Rev. B* **74**, 245322 (2006).
23. R. Zhu and M. Liu, *Eur. Phys. J. B* **89**, 2 (2016).
24. A. Branschädel, G. Schneider, and P. Schmittekert, *Ann. Phys. (Berlin)* **522**, 657 (2010).
25. U. Harbola, M. Esposito, and S. Mukamel, *Phys. Rev. B* **74**, 235309 (2006).
26. V. Moldoveanu, A. Manolescu, C.-S. Tang, and V. Gudmundsson, *Phys. Rev. B* **81**, 155442 (2010).
27. P. Myöhänen, A. Stan, G. Stefanucci, and R. van Leeuwen, *Europhys. Lett.* **84**, 67001 (2008).
28. P. Myöhänen, A. Stan, G. Stefanucci, and R. van Leeuwen, *Phys. Rev. B* **80**, 115107 (2009).
29. A.-P. Jauho, N. S. Wingreen, and Y. Meir, *Phys. Rev. B* **50**, 5528 (1994).
30. O. Shevtsov and X. Waintal, *Phys. Rev. B* **87**, 085304 (2013).

31. H. Haug and A.-P. Jauho, *Quantum Kinetics in Transport and Optics of Semiconductors* (Springer, Berlin, 2008).
32. J. Rammer, *Quantum Field Theory of Non-Equilibrium States* (Cambridge University Press, Cambridge, UK, 1997).
33. G. Stefanucci and R. van Leeuwen, *Nonequilibrium Many-Body Theory of Quantum Systems: A Modern Introduction* (Cambridge University Press, Cambridge, UK, 2013).
34. M. Di Ventra, *Electrical Transport in Nanoscale Systems* (Cambridge University Press, Cambridge, UK, 2008).
35. S. Datta, *Quantum Transport: Atom to Transistor* (Cambridge University Press, Cambridge, UK, 2005).
36. Y. Zhu, J. Maciejko, T. Ji, H. Guo, and J. Wang, *Phys. Rev. B* **71**, 075317 (2005).
37. J. Maciejko, J. Wang, and H. Guo, *Phys. Rev. B* **74**, 085324 (2006).
38. Y. Xing, B. Wang, and J. Wang, *Phys. Rev. B* **82**, 205112 (2010).
39. E. C. Cuansing and G. Liang, *J. Appl. Phys.* **110**, 083704 (2011).
40. D. Kienle, M. Vaidyanathan, and F. Léonard, *Phys. Rev. B* **81**, 115455 (2010).
41. M. P. Anantram and S. Datta, *Phys. Rev. B* **51**, 7632 (1995).
42. G. Platero and R. Aguado, *Phys. Rep.* **395**, 1 (2004).
43. A. Crépieux, F. Šimkovic, B. Cambon, and F. Michelini, *Phys. Rev. B* **83**, 153417 (2011).
44. A. Croy and U. Saalman, *Phys. Rev. B* **80**, 245311 (2009).
45. B. Dong, G.-H. Ding, and X. L. Lei, *J. Phys.: Condens. Matter* **27**, 205303 (2015).
46. G.-H. Ding, B. Xiong, and B. Dong, *J. Phys.: Condens. Matter* **28**, 065301 (2016).
47. W. H. Press, S. A. Teukolsky, W. T. Vetterling, and B. P. Flannery, *Numerical Recipes: The Art of Scientific Computing* (Cambridge University Press, Cambridge, UK, 2007).
48. E. C. Cuansing and J.-S. Wang, *Phys. Rev. B* **81**, 052302 (2010).
49. M. F. Ludovico, J. S. Lim, M. Moskalets, L. Arrachea, and D. Sanchez, *Phys. Rev. B* **89**, 161306(R) (2014).
50. Computer program FFTW version 3.3.4 2014 ([www.fftw.org](http://www.fftw.org)).
51. S. Datta, *Electronic Transport in Mesoscopic Systems* (Cambridge University Press, Cambridge, UK, 1995).